Establishing Quantitative Understanding of Energy Transfer to High Frequency in Nonlinear Dispersive Equations

Keagan G. Callis
University of Minnesota, Twin Cities

May 1st, 2017

Abstract

We present a family of particular solutions to a Hamiltonian system which was derived to study energy transfer to higher Fourier modes in solutions to the cubic defocusing nonlinear Schrödinger equation. The solutions in this family are not direct solutions to this nonlinear Schrödinger equation, but instead approximate solutions which transfer energy to higher Fourier modes. Our numerical work follows and expands upon work done in [4] and [8], where the existence of solutions exhibiting these properties was proven non-constructively. The solutions presented here depend heavily upon phase interactions in the Hamiltonian system, which has previously been poorly understood.

Contents

1 Introduction

In [4], a model Hamiltonian system was derived to approximate solutions to the following nonlinear Schrödinger equation:

$$\left.\begin{aligned} -i\partial_t u + \Delta u - |u|^2 u = 0 \\ u(0,x) = u_0(x) \end{aligned}\right\} \tag{1}$$

where $u(t,x)$ is complex valued and x is in the two dimensional torus $\mathbb{T}^2 := \mathbb{R}^2/(2\pi\mathbb{Z})^2$.

The model Hamiltonian system was derived in order to study the components of the bounded energy of finite energy solutions to (1), and was used to prove the existence of solutions to (1) whose energy components shift to higher Fourier modes. The system is referred to by the authors of [4] as the 'Toy Model' and is given by the following N dimensional complex Hamiltonian ([8]):

$$h(\mathbf{b}) = \sum_{j=1}^{N} \frac{1}{4}|b_j|^4 - \frac{1}{2}(b_j^2\overline{b_{j-1}}^2 + \overline{b_j}^2 b_{j-1}^2) \tag{2}$$

along with the symplectic form

$$d\omega = \frac{i}{2} db_j \wedge \overline{b_j}. \tag{3}$$

With (2) and (3) we have the following $2N$ differential equations:

$$\left.\begin{aligned} \dot{b}_j &= -2i\frac{\partial H}{\partial \bar{b}_j} \\ \dot{\bar{b}}_j &= 2i\frac{\partial H}{\partial b_j} \end{aligned}\right\} \tag{4}$$

where $0 \leq j \leq N+1$ and $b_0 \equiv b_{N+1} \equiv 0$.

This paper is concerned with solutions to the Toy Model (not with direct solutions to (1)). Thus for clarity and to provide a frame of reference we begin with a brief overview of why the Toy Model was derived and how it relates to (1).

To begin with, solutions to (1) with smooth initial data $u_0(x)$ (which are the solutions we consider in this paper) have two conserved quantities ([3], [9]), which are the Hamiltonian

$$E[u] := \int_{\mathbb{T}^2} \frac{1}{2}|\nabla u|^2 + \frac{1}{4}|u|^4 dx \tag{5}$$

and the Mass

$$\int_{\mathbb{T}^2} |u|^2 dx \tag{6}$$

which is also the $L^2(\mathbb{T}^2)$ norm of u.

Before we go further, we must first discuss the method by which the energy distribution of solutions to (1) was examined in [4] and by which the energy distribution will be examined in this paper, as doing this will enable a more quantitative discussion.

A natural way to measure the energy distribution of a solution is by measuring what is called its 1-Sobolev norm (also called its Energy norm). This is defined as

$$||u(t,\cdot)||_{H^1(\mathbb{T}^2)} = ||u(t)||_{H^1(\mathbb{T}^2)} = \Big[\sum_{n\in\mathbb{Z}^2} \langle n\rangle^2 |\hat{u}(t,n)|^2\Big]^{1/2}, \tag{7}$$

where $\langle n\rangle^2 = (1+|n|^2)$ and

$$\hat{u}(t,n) = \frac{1}{(2\pi)^2}\int_{\mathbb{T}^2} u(t,x)e^{-in\cdot x}dx, \tag{8}$$

which is the n^{th} Fourier coefficient obtained when one calculates the two-dimensional Fourier series of $u(t,x)$.

This is a natural norm to consider when studying the frequency components of a solution since it takes into account the influence of all frequency components in a solution. Additionally, this is a particularly natural norm to consider for this problem for the following reason: the two conserved quantities (5) and (6) imply that the 1-Sobolev norm is uniformly bounded above by some constant value. This implies that we cannot find finite-energy solutions whose frequency components grow arbitrarily.

However, the $\hat{u}(t,n)$ which primarily contribute to a solution's 1-Sobolev norm is something which can vary. What we are interested in then are solutions which begin with their 1-Sobolev norm obtaining most of its value from $\hat{u}(t,n)$ with low $|n|$ and after some time have their 1-Sobolev norm obtain most of its value from $\hat{u}(t,n)$ with high $|n|$. To measure this shift, the following s-Sobolev norm is defined:

$$||u(t,\cdot)||_{H^s(\mathbb{T}^2)} = ||u(t)||_{H^s(\mathbb{T}^2)} = \Big[\sum_{n\in\mathbb{Z}^2} \langle n\rangle^{2s} |\hat{u}(t,n)|^2\Big]^{1/2}. \tag{9}$$

Thus, in this notation, we are interested in finding solutions to (1) for which (9) grows for $s > 1$. To borrow terminology from [4], we denote this shift in frequency components a 'norm explosion.'

A summary of how the Toy Model relates to (1) is given in Section 2, along with

some of the properties which the Toy Model possesses. An important property which we mention now is that if a solution $\mathbf{b}(t)$ to the Toy Model begins with the majority of its magnitude concentrated in its components at lower indices and after some time has the majority of its magnitude concentrated in its components at higher indices, the corresponding solution to (1) which $\mathbf{b}$ approximates will have the following property: the solution's 1-Sobolev norm will initially obtain most of its value from its components at lower indices and after some time will obtain most of its value from its components at higher indices.

Indeed, an important result of [4] is the derivation of a solution to the Toy Model which transfers its magnitude from lower indices to higher indices in finite time. This result then implies the existence of solutions to (1) whose energy components shift to higher Fourier modes in finite time. The main result of [4] is summed up in the following theorem:

Theorem 1 *(cf. [4]) Let* $1 < s$, $K \gg 1$, *and* $0 < \delta \ll 1$ *be given parameters. Then there exists a global smooth solution* $u(t,x)$ *to (1) and a time* $T > 0$ *with*

$$||u(0)||_{H^s} \leq \delta$$

and

$$||u(T)||_{H^s} \geq K.$$

The overall goal to which this paper and previous work ([4], [8], [5], [7]) contributes is to work towards an answer to the question posed by Bourgain ([1], [2]) which asks if there exist solutions to (1) with initial data $u_0 \in H^s$ for $s > 1$ such that

$$\limsup_{t\to\infty} ||u(t)||_{H^s} = \infty \tag{10}$$

Indeed, Theorem 1 immediately gives the following result

$$\inf_{\delta>0}\left\{\limsup_{t\to\infty}\Big(\sup_{||u_0||_{H^s}\leq\delta}||u(t)||_{H^s}\Big)\right\} = \infty, \tag{11}$$

which is in some sense close to (10), but in others falls short.

The purpose of this paper is to present a family of solutions to (2) which have the same norm explosion property as the solution derived in [4] and to report on what observations led to the discovery of this family. The beginning of the numerical work was based on work done in [5], and some of the first solutions to the Toy Model we examined were solutions first examined in [5].

Of interest is that the solutions presented here rely heavily on the interactions between the phases of adjacent b_k (where the word 'phase' here is used in the complex variable sense), the utility of which was not observed in previous work ([4], [8]).

Two other interesting properties of these solutions are the following: the first is that after their magnitude has been transferred through a collection of indices, the difference between adjacent phases remains the same (up to small errors), and the second is that there is a constant 'drift' in the phases - that is, the phases decrease linearly in time (in addition to their other dynamics).

2 Properties of the Toy Model

To begin this section, we first briefly summarize how the Toy Model was derived and how it relates to (1). We then proceed to mention a few of the properties of the Toy Model which are relevant for this paper.

The first step in deriving (2) is to view (1) in terms of the following Fourier expansion:

$$u(t,x) = \sum_{n\in\mathbb{Z}^2} a_n(t)e^{in\cdot x+|n|^2 t} \tag{12}$$

In this frame, after utilizing gauge freedom to cancel out certain interactions, one can obtain the following evolution of a_n:

$$\begin{aligned} -i\partial_t a_n = &- a_n|a_n|^2 + \\ &\sum_{(n_1,n_2,n_3)\in\Gamma(n)} a_{n_1}\overline{a_{n_2}}a_{n_3}e^{i\omega_4 t} \end{aligned} \tag{13}$$

where

$$w_4 = |n_1|^2 - |n_2|^2 + |n_3|^2 - |n|^2 \tag{14}$$

and

$$\begin{aligned} \Gamma(n) = \{&(n_1,n_2,n_3)\in(\mathbb{Z}^2)^3 : \\ &n_1 - n_2 + n_3 = n, \\ &n_1 \neq n, n_3 \neq n\} \end{aligned} \tag{15}$$

Now, the terms in this summation which contribute the most to the solution will be those without the factor $e^{i\omega_4 t}$. These are precisely the terms whose (n_1,n_2,n_3) are in the following *resonant set*:

$$\begin{aligned} \Gamma_{res}(n) = \{&(n_1,n_2,n_3)\in\Gamma(n) : |n_1|^2 - |n_2|^2 \\ &+ |n_3|^2 - |n|^2 = 0\}. \end{aligned} \tag{16}$$

From here, we have the following:

$$-\partial_t r_n = -r_n|r_n|^2 + \sum_{(n_1,n_2,n_3)\in\Gamma_{res}(n)} r_{n_1}\overline{r_{n_2}}r_{n_3} \tag{17}$$

The next step taken in [4] is the construction of a frequency set Λ which is the union of N different disjoint generations Λ_k. These generations have a number of properties which are given in [4]. One of the consequences of these properties is that for each generation, we have the following:

$$r_n(t) = r'_n(t),\ \forall n,n'\in\Lambda_k \tag{18}$$

Finally, we have that the relation between the components of $\mathbf{b}$ in the Toy Model to (1) is

$$b_k(t) = r_n(t),\ \forall n\in\Lambda_k. \tag{19}$$

The Toy Model (2) enjoys a number of properties. A more complete list is given in [4], but in this paper we shall only be interested in a few of these.

The first is that this system has two conserved quantities (also called 'first integrals'): The Hamiltonian itself, which we denote to be the Energy of the system, and the Mass, which we define by

$$M(\mathbf{b}) = \sum_{j=1}^{N} |b_j|^2. \tag{20}$$

We also refer to $|b_j|^2$ as the Mass contained in b_j.

Another property that the Toy Model possesses is that if $b_k(t) = 0$ for some t, then $b_k(t) = 0$ for all time, and the Mass of $\mathbf{b}$ will never be able to be transferred past this index. This is due to the fact that the derivative of each b_k is proportional to the value of b_k.

Related to this is the fact that the Toy Model also has the following periodic orbits which, following [4], we label T_j:

$$b_j(t) = e^{-it},\ b_k = 0 \text{ for all } k\neq j \tag{21}$$

Accompanying the periodic orbits (21), there exist heteroclinic orbits which connect two adjacent T_j together. It is useful to mention

these heteroclinic orbits because the solutions constructed in past work ([4] and [8]) utilize these orbits in order to transfer Mass from one index to the next. More precisely stated, the solutions constructed in previous work travel close to these heteroclinic orbits one after the other in order to continually shift Mass from one index to the next. This causes the solutions to have the majority of their Mass concentrated in a single index at a given time (or distributed between two adjacent indices).

The solutions constructed in this paper also have their Mass concentrated in just a single index at a given time (or distributed between two adjacent indices). Despite this, it is unknown if the solutions in this paper transfer Mass using the same mechanisms that the solutions constructed in previous work use.

The last property we mention is the following: if one adds a constant to the phase of every component of $\mathbf{b}$, the dynamics which are induced by (2) remain unchanged. This is due to the fact that the quantity which appears in this system's differential equations (see (25)) is the difference between adjacent phases - not the actual values of the phases. Furthermore, this immediately implies that the constant drift in the phases of the solutions presented does not directly affect their dynamics.

3 Modifying the Toy Model

In this section we make some preliminary modifications to the Toy Model for ease of discussion.

Following previous work ([4], [8]), to make the phase interactions more apparent we first perform the following transformation on $\mathbf{b}$:

$$b_j(t) = \sqrt{r_j(t)}e^{i\theta_j(t)} \tag{22}$$

Doing so yields the following Hamiltonian:

$$h(\mathbf{b}) = \sum_{j=1}^{N} \frac{1}{4}r_j^2 - r_j r_{j-1}(\cos\left(2(\theta_j - \theta_{j-1})\right)) \tag{23}$$

with the symplectic form

$$d\omega = \frac{1}{2}dr_j \wedge d\theta_j. \tag{24}$$

These then yield the following system of differential equations:

$$\begin{aligned}\dot{\theta}_j = &-r_j + 2r_{j-1}\cos\left(2(\theta_j - \theta_{j-1})\right) \\ &+2r_{j+1}\cos\left(2(\theta_{j+1} - \theta_j)\right)\end{aligned} \tag{25}$$

$$\begin{aligned}\dot{r}_j = &4r_j r_{j-1}\sin\left(2(\theta_j - \theta_{j-1})\right) \\ &-4r_{j+1}r_j\sin\left(2(\theta_{j+1} - \theta_j)\right)\end{aligned} \tag{26}$$

Adding to the simplification of this system beyond that done in [4], we first note that since the trigonometric functions involved are 2π periodic, and each has a factor of 2 multiplying the difference between two adjacent indices, we may safely take each θ_j's value modulo π instead of the usual modulo 2π.

We then define the following:

$$\phi_j = 2\theta_j \tag{27}$$

which is taken modulo 2π, and we obtain the following system of differential equations:

$$\begin{aligned}\dot{\phi}_j = &-2r_j + 4r_{j-1}\cos\left(\phi_j - \phi_{j-1}\right) \\ &+4r_{j+1}\cos\left(\phi_{j+1} - \phi_j\right)\end{aligned} \tag{28}$$

$$\begin{aligned}\dot{r}_j = &4r_j r_{j-1}\sin\left(\phi_j - \phi_{j-1}\right) \\ &-4r_{j+1}r_j\sin\left(\phi_{j+1} - \phi_j\right)\end{aligned} \tag{29}$$

The Mass in this system is now given by

$$M(\mathbf{b}) = \sum_{j=1}^{n} r_j \tag{30}$$

and the Energy given by (23).

We shall use the Mass and the Energy of our solutions as an indication of their accuracy, as exact solutions would conserve these quantities.

4 Initial Data

To begin the discussion on the initial data used for the solutions to (2) which approximate norm-explosion solutions to (1), we first present the initial data and then proceed to discuss the properties it induces in solutions and the motivations which led to these initial data.

For some N equal to the dimension of the Toy Model and j denoting where the Mass begins, we have the following initial values:

Table 1: Initial Data

Variable	Value at $t = 0$
ϕ_k, $1 \leq k \leq j-2$	Any value between 0 and 2π
ϕ_{j-1}	$\sigma\pi$
ϕ_j	0
ϕ_{j+1}	$-\sigma\pi$
ϕ_k, $j+2 \leq k \leq N$	$(1/2)\pi$ if $j-k$ is odd $(3/2)\pi$ if $j-k$ is even
r_j	L
r_{j-1} *and* r_{j+1}	δ
r_k, $1 \leq k \leq j-2$ $j+2 \leq k \leq N$	ϵ

with typical values (which were obtained through trial and error for $N = 100$) of $\delta = 0.01$, $\epsilon = 0.0004$, $\sigma = 1.35$, and $L = 1$. The exact relation between these values which produces the desired growth in the solutions is currently unknown.

Also note that this model of initial data has been found to work for any value of N, with appropriate values of the parameters - that is, if a set of parameters works for some N, then we have found that the same set of parameters works for other N as well.

Using these data, the Mass is initially concentrated in r_j. After some period (around 2.5 seconds with the values given after Table 1), the solutions then resemble this initial data except with the j index shifted to $j+1$ and with π added to each phase, up to small deviations in every term. These deviations are sufficiently small such that the solution then repeats this process until the index containing the majority of the Mass reaches N, after which one of two things occurs: either the solution will 'reflect' and will start to descend (transfer Mass backwards) down to lower indices, or it will stop transferring Mass in an orderly fashion and instead do what we elegantly define as 'get stuck', which means it will continually and unorderedly distribute the majority of its Mass among a handful of nodes.

We provide an example of a solution with these initial data in Figure 1 using the following values: $N = 100$, $j = 3$, $\delta = 0.01$, $\epsilon = 0.0013$, and $\sigma = 1.35$. The numerical method used here (and for all plots of solutions) was the Runge-Kutta Prince-Dormand method (see [6]) on MATLAB, with a relative error tolerance of 10^{-12} and an absolute error tolerance of 10^{-15}. In this solution, the traveling wave reaches the end and then does what we defined as 'gets stuck'. The reason this solution gets stuck is because the deviations of each term from matching Table 1 become large enough such that the wave does not continue to transfer its mass according to orderly dynamics induced in data matching Table 1.

Also apparent in Figure 1 is the intriguing observation that after a solution travels through a set of indices, the phases at these

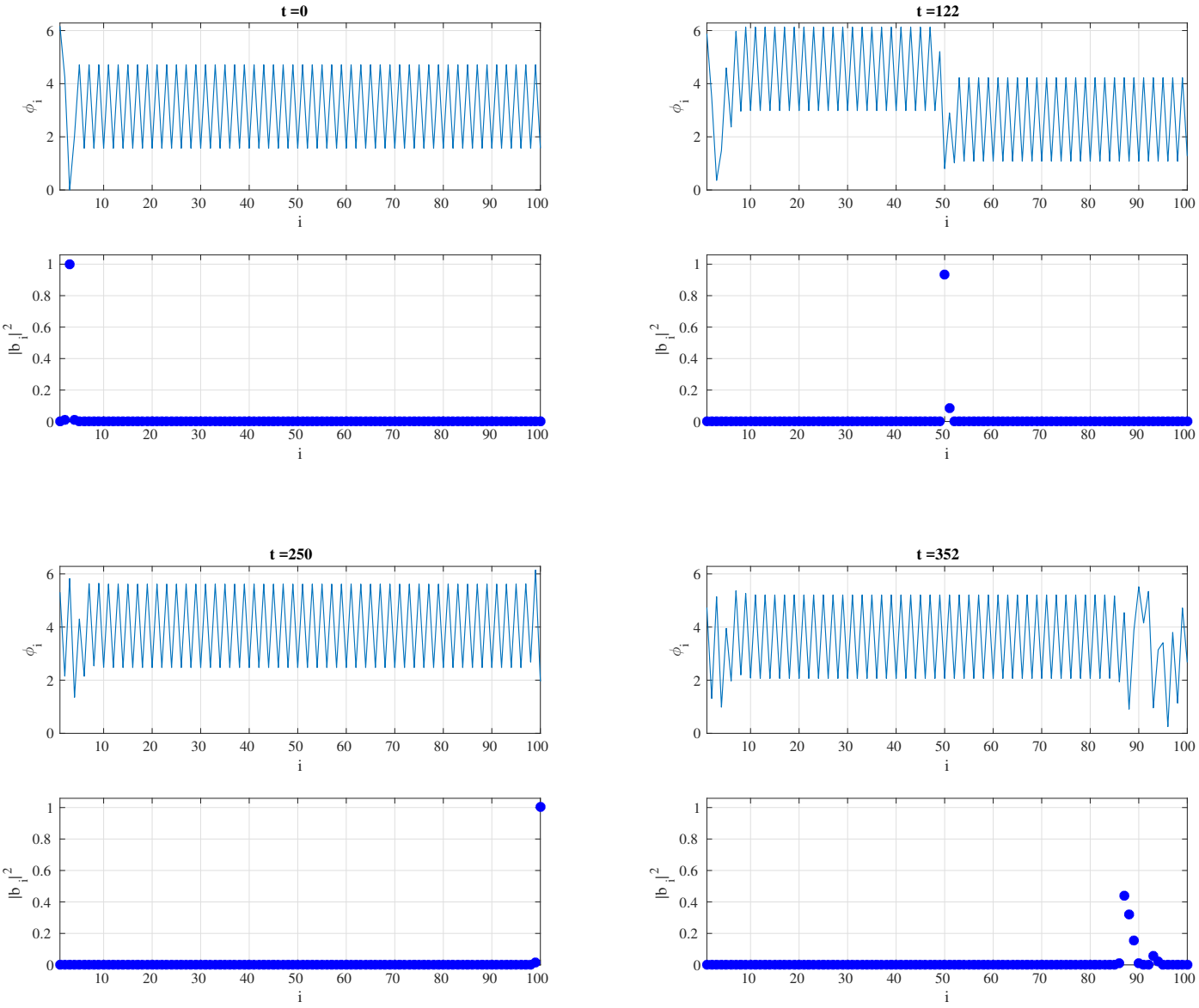

Figure 1: A solution to the Toy Model which transfers Mass from $j = 3$ to $j = N$. The initial data is given by Table 1 with the following values: $N = 100$, $j = 3$, $L = 1$, $\delta = 0.01$, $\epsilon = 0.0004$, and $\sigma = 1.35$. The plots show the solution at various times, and include the phase at each index on the top and the Mass at each index on the bottom of each plot. As can be seen, after $t = 250$, the solution begins to travel back down but by $t = 352$, the solution exhibits the phenomena we termed 'gets stuck.'

indices are left with a difference of π between each adjacent phase. Further, depending on the values of the parameters in Table 1, the difference between the phases at indices the wave has already traveled through and the phases at indices the wave has not yet traveled through can vary. The exact relation between the parameters in Table 1 and this difference is currently unknown.

As for the motivation for searching for initial data like those described in Table 1, we first describe what led to the motivation of setting each phase to a constant value depending on its parity. The following discussion uses the differential equations given in (25) and (26) rather than those given in (28) and (29), as the simplification (27) (i.e. the idea of taking θ to be π periodic instead of 2π periodic) had not been developed.

Initially, following [5], solutions with Mass distributed as described in Table 1 and with completely random phases between 0 and 2π in each index were run various times. There was no consistent observation of ordered growth of these solutions, so we moved on to observing solutions with the same Mass distribution but with random phases between 0 and some maximum less than 2π. In this case, the solutions appeared to travel further when this maximum was around $\pi/2$.

This observation, along with the knowledge that what influences the dynamics is the difference between two adjacent phases rather than their actual value led to the inference that it was a difference of some value around $\pi/2$ between two adjacent phases which contributed to growth. Thus, the idea of setting θ_k at every other index exactly to $\pi/2$ while leaving the rest 0 was attempted, and the desired growth was more consistently observed. It was also observed that only the phases at indices greater than j needed to alternate between $\pi/2$ and 0, and the rest could remain unspecified (i.e. have random values between 0 and 2π).

Finally, the idea of setting the phase of the j index to 0 and the two adjacent phases to values different from 0 and $\pi/2$ was from examining the tables of initial data in [4]. To describe how we used the information from these tables to refine our solutions requires a brief overview of some of the analysis performed in [4].

To begin with, In [4] the authors perform a transformation from $\mathbf{b}$ in (2) to what they label $\mathbf{c}$. This transformation is defined by:

$$b_j = re^{i\theta};\ c_k = b_k e^{-i\theta} = \sqrt{r_k} e^{i(\theta_k - \theta)} \text{ for } k \neq j. \tag{31}$$

This is done so that the phase of each c_k is equal to the difference between the phases of b_k and b_j. The authors also perform the following transformation on $c_{j\pm1}$ to obtain $c_{j\pm1}$ in terms of the real numbers $c^-_{j\pm1}$ and $c^+_{j\pm1}$:

$$c_{j\pm1} = \omega c^-_{j\pm1} + \omega^2 c^+_{j\pm1} \tag{32}$$

where $\omega = e^{2i/3}$ is a cube root of unity.

They later proceed to give the following configuration of the magnitudes of c_k when their solution has its Mass concentrated in b_j:

Table 2: Data from [4]

$c_{\leq j-2}$	ϵ^2
c^-_{j-1}	ϵ
c^+_{j-1}	ϵ^3
c^-_{j+1}	ϵ^3
c^+_{j+1}	ϵ
$c_{\geq j+2}$	ϵ^2

where ϵ is a small number.

At this point in the analysis done in [4], they no longer consider the phases at each index - thus we are free to decide what they may be.

Using Table 2, we translate back into b_k and add phases in accordance with the observation that setting the phase at each odd index to $\pi/2$ and the phase at each even index to 0 seems to consistently produce a traveling wave. Doing so yields the following:

Table 3: Initial Data

Variable	Value at $t = 0$
ϕ_k, $1 \leq k \leq j-2$	Any value between 0 and 2π
ϕ_{j-1}	$\sigma\pi$
ϕ_j	0
ϕ_{j+1}	$-\sigma\pi$
ϕ_k, $j+2 \leq k \leq N$	π if $j-k$ is odd 0 if $j-k$ is even
r_j	L
r_{j-1} *and* r_{j+1}	$\epsilon^2 - \epsilon^4 + \epsilon^6$
r_k, $1 \leq k \leq j-2$ $j+2 \leq k \leq N$	ϵ^2

where $\sigma = \dfrac{2\arctan\left(\sqrt{3}\left(\dfrac{\epsilon^3-\epsilon}{\epsilon^3+\epsilon}\right)\right)}{\pi}$ and $L = (1 - \sum_{k\neq j} r_k)$. Note that this value of L comes from the fact that the total Mass of the solution constructed in [4] is 1. Also note that if we take the limit as ϵ goes to 0, we obtain $\sigma = (4/3)$, which is close to the value of 1.35 used in the typical data given after Table 1.

One observation we make here is that the Mass contained at the indices adjacent to the j^{th} index is lower in Table 3 (compared to the Mass at the other indices) than in typical values for Table 1.

Using this initial data, we were able to consistently obtain traveling wave solutions after finding suitable values of ϵ depending on N. However, it was then observed is that if we begin with initial data given by Table 3, the solutions will consistently arrange themselves to resemble data given by Table 1 after a few transfers of Mass between indices.

To illustrate this phenomena, we include in Figure 2 a plot of the evolution of the phases using initial data from Table 3, and show that after a few transfers of Mass between indices the data resembles that given by Table 1.

The rest of the refinements on the data going from Table 3 to Table 1 were obtained through trial and error.

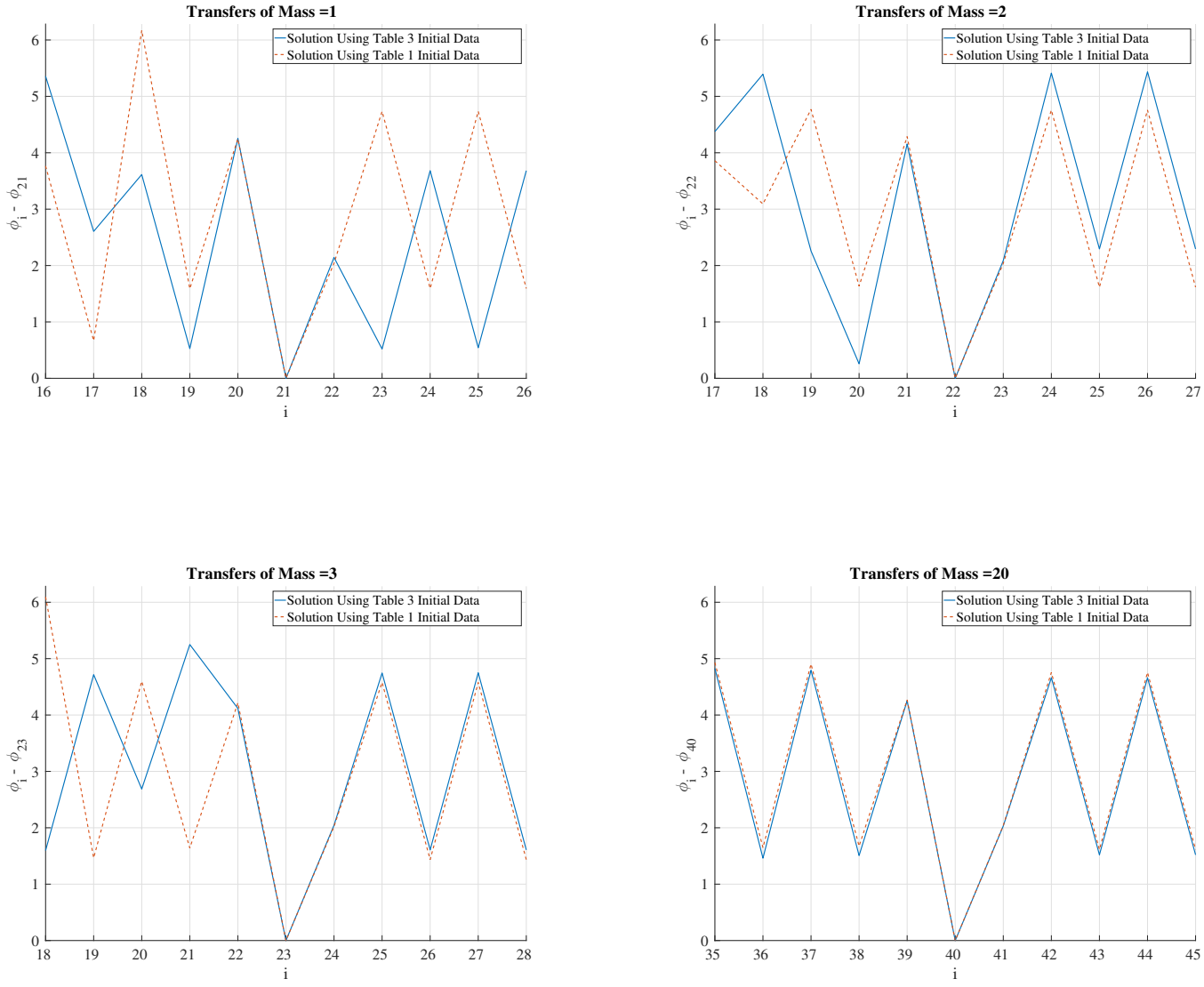

Figure 2: Plots comparing the phases of a solution using initial data given in Table 3 with $j = 20$, $\epsilon = 0.035$ to a solution using initial data given in Table 1 with $j = 20$, $\epsilon = 0.0015$, $\delta = 0.0102$, $\sigma = 1.35$, and $L = 1$. The plots are shown for times when the solution has its Mass peaked in one index. The top left graph is at the time when the Mass is peaked in the 21^{st} index, the top right graph has the Mass peaked in the 22^{nd} index, the bottom left has the Mass peaked in the 23^{rd} index, and the bottom right graph has the Mass peaked in the 40^{th} index. Notice that the solution's data begins to match that given by Table 1 after some transfers of Mass.

5 Observations of the Solutions

Following [5], we also define the following indicator norms:

$$||\mathbf{b}||_{h^s}^2 = \sum_{j=1}^{N} j^{2s} r_j \tag{33}$$

which we use as a way to measure the shift of the Mass in solutions to higher modes. Since the Mass shifting to higher modes implies that the approximated solution to (1) grows in its s-Sobolev norm for s ¿ 1, growth in this indicator norm roughly implies growth in the approximated solution's s-Sobolev norm. The exact relation of this norm to the s-Sobolev norm is complicated, however - to observe the exact s-Sobolev norm's growth would require what is called the placement function described in [4], which was non-constructively proved to exist.

The growth in this indicator norm for s=2 is shown in Figure 3 for the same data used in Figure 1.

We also plot the Mass and Energy of this same solution in Figures 4 and 5, respectively. Small deviations in both of these is observed, though in the Energy it can be seen that after the solution gets stuck, there is more deviation than before. This is indicative of our solution losing some degree of accuracy after this point, though the deviation remains small enough that our solutions are still accurate.

To begin the discussion of our observations of the characteristics of the solutions, we note that there is a constant, nearly-linear decrease in the phase of each index. This can be explained by simply plugging in the initial data from Table 1 into (28). Doing so yields the initial values of the derivatives of the phases as given in Table 4

Table 4: Initial Speed of the Phases

Variable	Value at $t = 0$
$\dot{\phi}_N$	-6ϵ
$\dot{\phi}_k$, $1 \leq k \leq j-3$	$\mathcal{O}(\epsilon)$
$\dot{\phi}_k$, $j+3 \leq k \leq N-1$	-10ϵ
$\dot{\phi}_{j-2}$	$4\delta \cos(\sigma\pi - \frac{\pi}{2}) + \mathcal{O}(\epsilon)$
$\dot{\phi}_{j-1}$	$-2\delta + 4\epsilon \cos(\sigma\pi - \frac{\pi}{2})$ $+4L \cos(\sigma\pi)$
$\dot{\phi}_j$	$-2L + 8\delta \cos(\sigma\pi)$
$\dot{\phi}_{j+1}$	$-2\delta + 4\epsilon \cos(\sigma\pi + \frac{3\pi}{2})$ $+4L \cos(\sigma\pi)$
$\dot{\phi}_{j+2}$	$-6\epsilon + 4\delta \cos(\sigma\pi + \frac{3\pi}{2})$

As can be readily seen, there is initially a constant decrease of 10ϵ in almost every term, with the exceptions being the terms surrounding the j index, the terms before the j index, and the last index.

The slightly different decrease in the last index causes the phases at the last couple of indices to deviate non-negligibly from Table 1 given a long enough time. To illustrate this, Figure 6 contains the solution with initial data $N = 1000$, $j = 3$, $L = 1$, $\delta = 0.01$, $\epsilon = 0.0013$,

and $\sigma = 1.35$. In this situation, the traveling wave is actually unable to completely reach the end, as the time it takes to travel that far is long enough such that by the time the wave nears the end the phases at the last indices have deviated too far from Table 1 and the traveling wave gets stuck.

Finally, we also include an example of data which undergoes reflection after reaching the last index. This is contained in Figure 7.

It is our opinion that this reflection however is uninteresting, as it is likely to be a

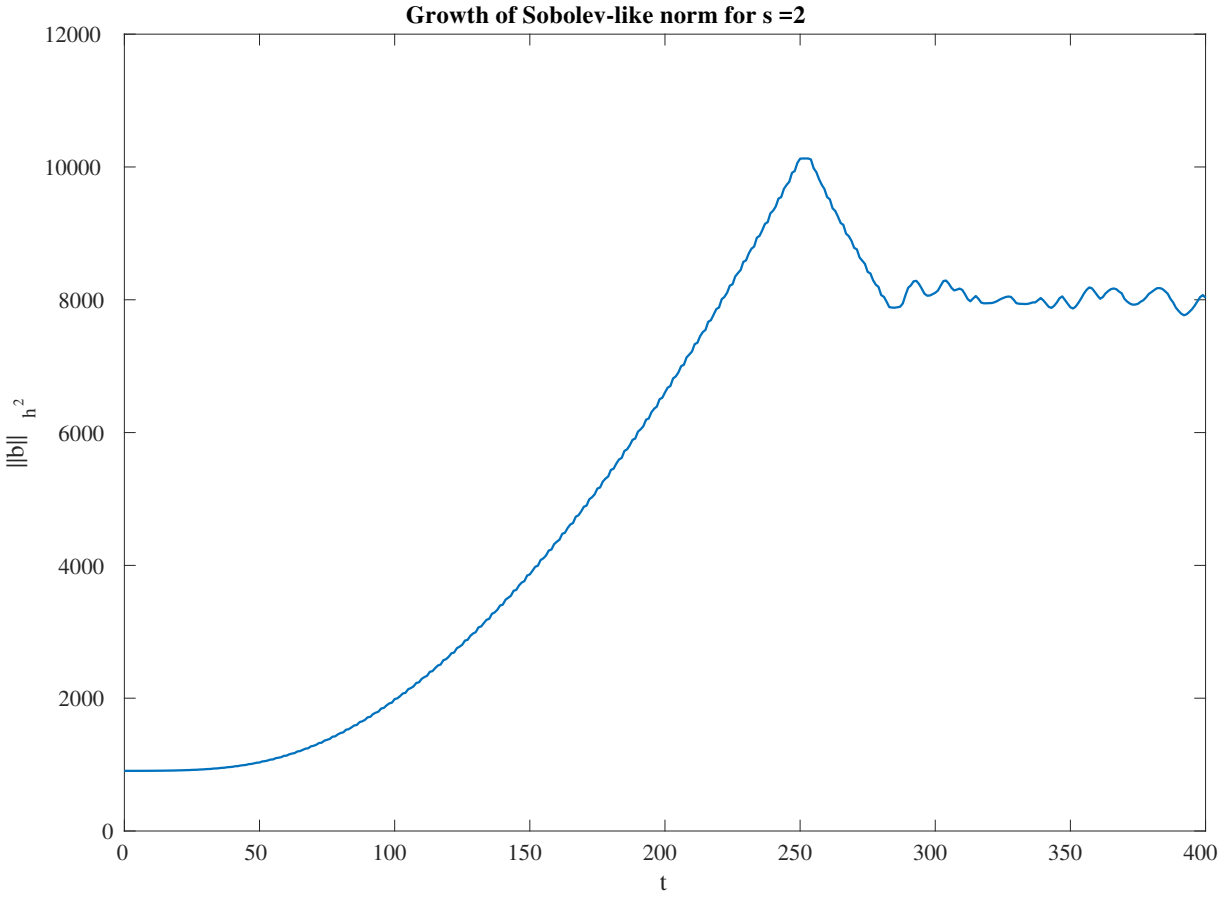

Figure 3: A plot of the growth in the indicator norm for s=2. The solution used to obtain this plot is the same as that used for Figure 1.

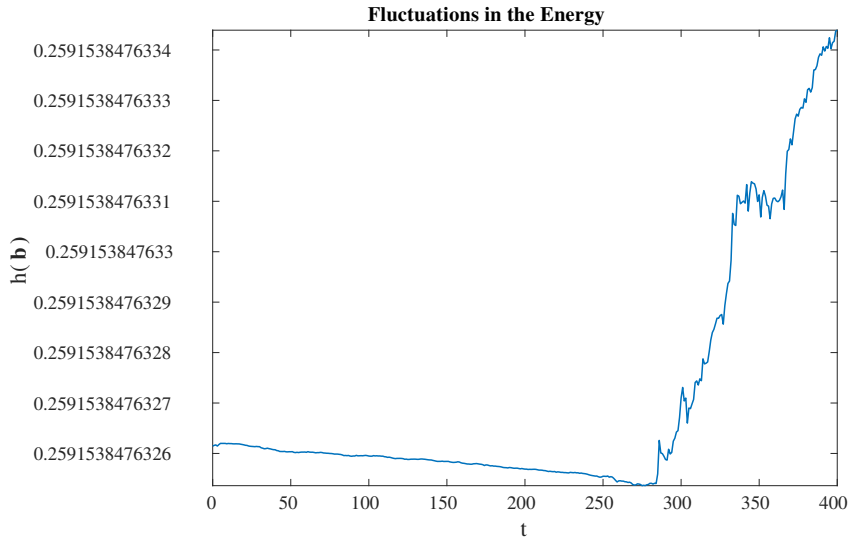

Figure 4: A plot showing the fluctuation in the Energy (23) of the solution used in Figure 1. Notice how after the solution gets stuck the fluctuation in the Energy changes drastically - however the overall variance in the Energy remains very small and hence indicates our solution remains accurate.

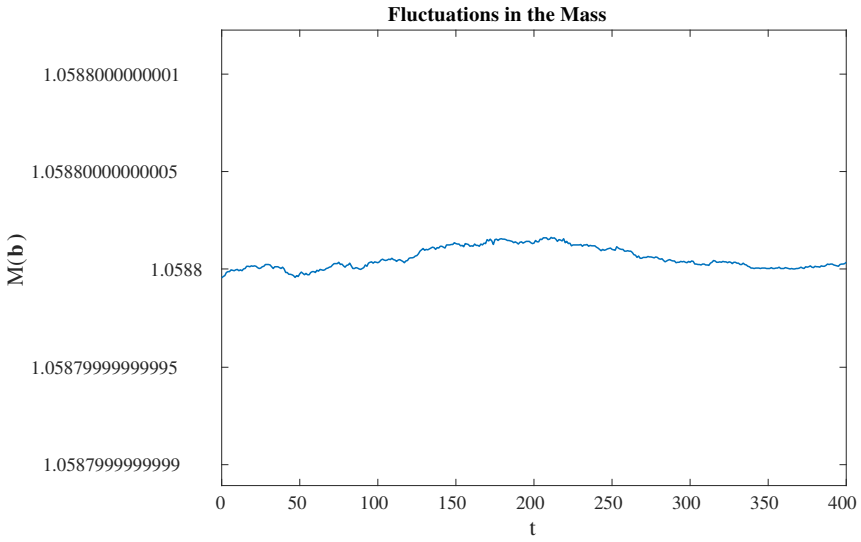

Figure 5: A plot showing the fluctuation in the Mass (30) of the solution used in Figure 1. Notice that it remains nearly completely constant, indicating that our solution is accurate.

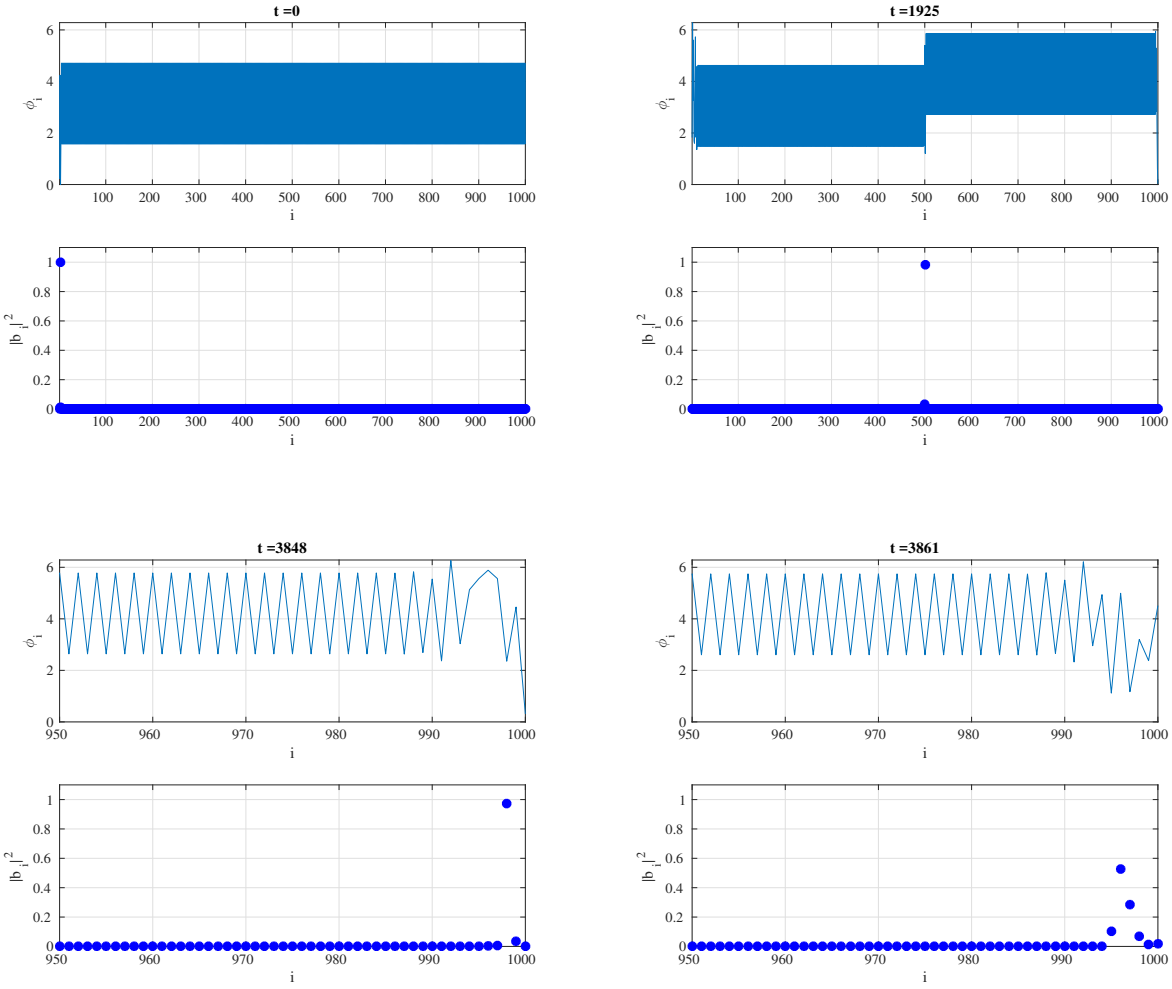

Figure 6: A solution to the Toy Model which transfers Mass from $j = 3$ to some index close to but not equal to $N = 1000$. The initial data is given by Table 1 with the following values: $N = 1000$, $j = 3$, $L = 1$, $\delta = 0.01$, $\epsilon = 0.0013$, and $\sigma = 1.35$. Note that for the bottom two plots, the indices shown are from 950 to 1000 in order to more clearly show that the solution is unable to transfer Mass all the way to the N^{th} index due to the large deviance in the last phases from matching Table 1. This large deviance can be intuitively explained by observing the different initial drift speed in the phase at the last index (compared to the -10ϵ speed in most of the other phases) as shown in Table 4.

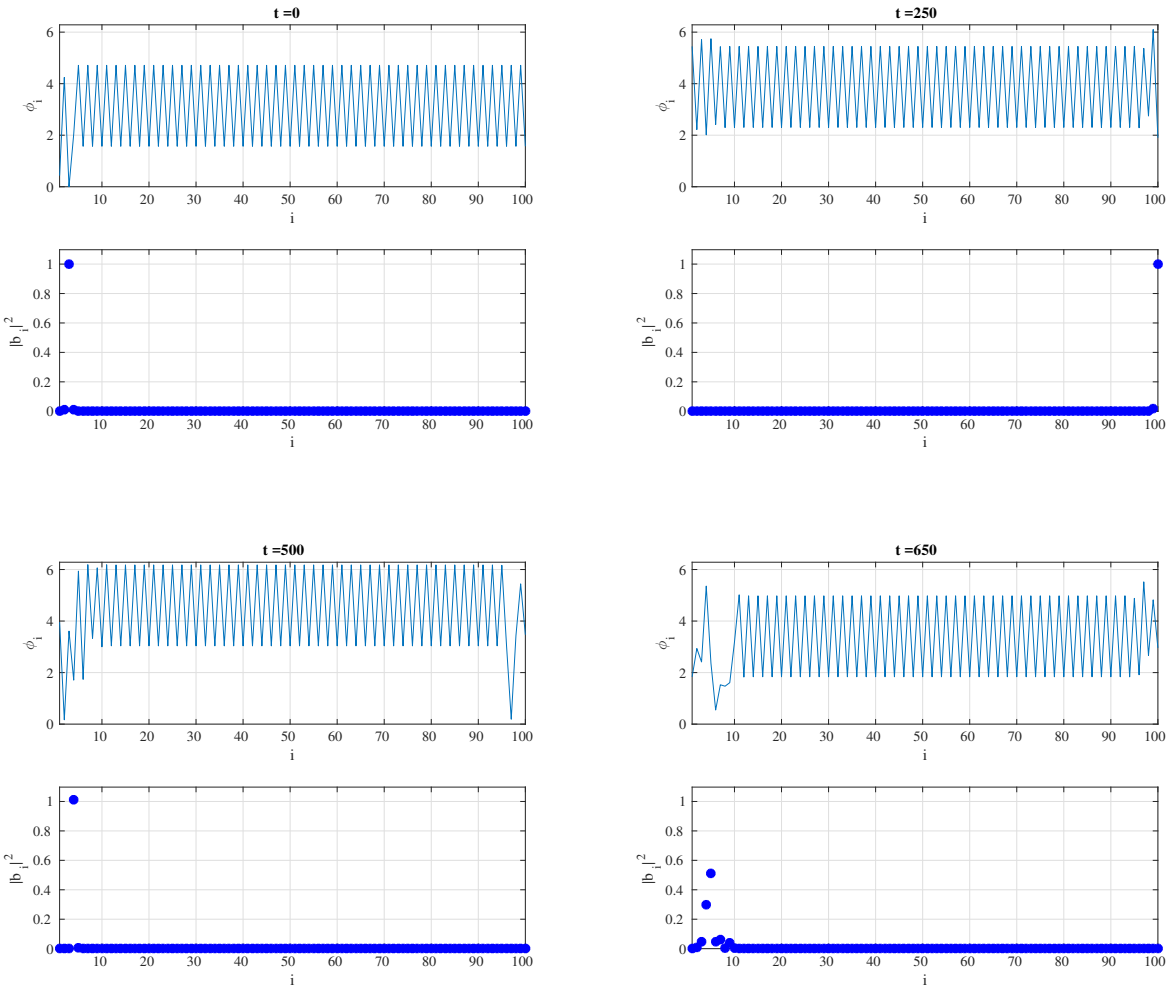

Figure 7: A solution to the Toy Model which reflects after transferring Mass from $j = 3$ to $j = 100$. After reflecting, the wave successfully travels back down to the third index, and continue traveling backwards to eventually reflect again off of the first index. By $t = 650$ the solution becomes stuck around $j = 5$. The initial data used for this wave was from Table 1 with $N = 100$, $j = 3$, $L = 1$, $\epsilon = 0.0008$, $\delta = 0.01$, and $\sigma = 1.35$.

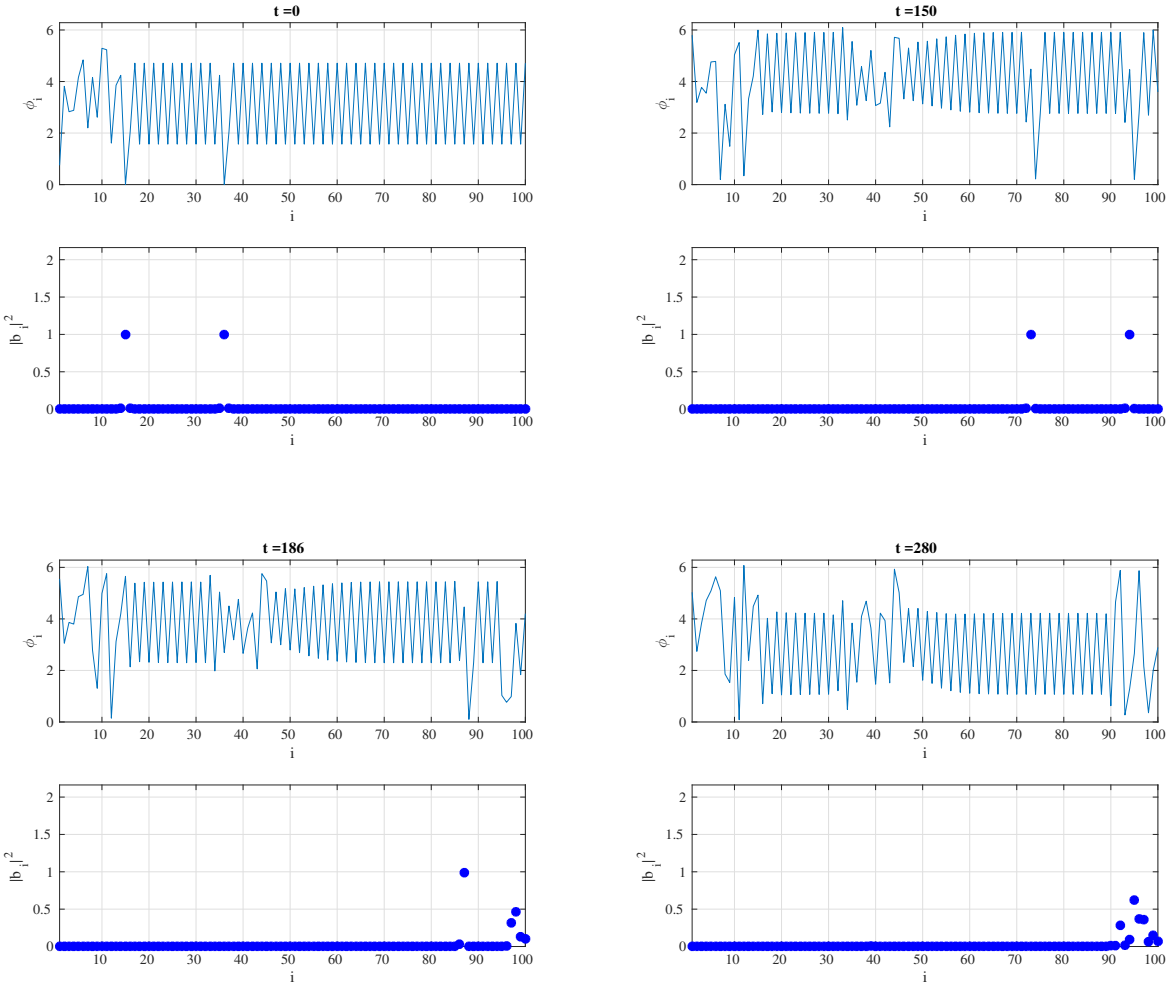

Figure 8: A solution to the Toy Model which transfers its Mass to higher indices via two wave packets. The initial data is given by Table 5, with $j_1 = 15$, $j_2 = 36$, and $N = 100$, $L = 1$, $\epsilon = 0.0013$, $\delta = 0.01$, and $\sigma = 1.35$. As can be seen from Table 5, the data around each of these indices resembles Table 1. Notice that there is some roughness when the lower-indexed packet first travels through the set of indices that the higher-index packet has traveled through, but that despite this the solution stabilizes and shows that after a wave has traveled through a set of indices, the indices are left in such a position that they prepared to transmit another packet.

side-effect of the more interesting fact that the data is such that after a wave has traveled through a set of indices, the phases are left with a difference of π between adjacent phases. That is, after a wave initially travels through the phases, the phases are left organized in such a way that they are ready to transmit another wave. Hence, we believe the fact that some waves travel back down is likely a mere coincidence which occurs when, after the solution hits the last phase, conditions happen to be just right that it begins to become transmitted again through the indices (this time going in reverse).

To support the claim that after a wave travels through a set of indices the phases remain ready to transmit another wave, we provide in Figure 8 a solution which transmits Mass via two wave packets. The initial data of this solution is given by Table 5.

Table 5: Initial Data used for Figure 8

Variable	Value at $t = 0$
ϕ_k, $1 \leq k \leq j_1 - 2$	Any value between 0 and 2π
ϕ_{j_1-1}	$\sigma\pi$
ϕ_{j_1}	0
ϕ_{j_1+1}	$-\sigma\pi$
ϕ_k, $j_1 + 2 \leq k \leq j_2 - 2$	$(1/2)\pi$ if $j_1 - k$ is odd $(3/2)\pi$ if $j_1 - k$ is even
ϕ_{j_2-1}	$\sigma\pi$
ϕ_{j_2}	0
ϕ_{j_2+1}	$-\sigma\pi$
ϕ_k, $j_2 + 2 \leq k \leq N$	$(1/2)\pi$ if $j_2 - k$ is odd $(3/2)\pi$ if $j_2 - k$ is even
r_{j_1} and r_{j_2}	$L = 1$
r_{j_1-1}, r_{j_1+1}, r_{j_2-1}, r_{j_2+1}	δ
r_k, $1 \leq k \leq j - 2$ $j + 2 \leq k \leq N$	ϵ

6 Conclusions

To conclude our report: we have presented a family of solutions (related to the data constructed in [4]) to the Toy Model (2) which shift Mass from lower indices to higher indices and thus approximate solutions to (1) which grow in finite time in their s-Sobolev norms for $s > 1$. The family presented differs from previous work ([4] and [8]) in that it incorporates explicitly the phase components of the variables in the Toy Model.

One possibility for further study would be to examine what exactly is the relation between the parameters given in Table 1 which produces growth in the solutions. Related to this, it would also be interesting to see what the relation is between these parameters and the difference in the phases before and after a wave travels through them.

Additionally, it would be interesting to relate the solutions to the Toy Model directly to solutions to (1) - that is, to find explicitly the placement function whose existence was proven in [4].

7 Acknowledgments

We would like to particularly thank professor Markus Keel for his invaluable insights into this area of study and for the introduction to both the nonlinear Scrödinger equation examined and the Toy Model. We also would like to thank Dr. Brittan Farmer for aid in some of the numerical work done here and Rajendra Beekie for helping review some earlier drafts of this paper.

References

[1] J. Bourgain, *Remarks on Stability and Diffusion in High-Dimensional Hamiltonian Systems and Partial Differential Equations* Ergodic Theory Dynam. Systems 24:5 (2004), **1331–1357**

[2] J. Bourgain, *Problems in Hamiltonian PDE's* Geom. Funct. Anal., Special Volume, Part I:**32–56**, 2000. GAFA 2000 (Tel Aviv, 1999).

[3] T. Cazenave, *An introduction to nonlinear Schrödinger equations*, Textos de Metodos Matematicos, **26**, 3rd Edition, 1996.

[4] J. Colliander, M. Keel, G. Staffilani, H. Takaoka, T. Tao *Transfer of Energy to High Frequencies in the Cubic Defocusing Nonlinear Schrödinger Equation*, Inventiones Math., **181**, 2010, 31–113.

[5] J. Colliander, J. Marzuola, T. Oh, G. Simpson *Behavior of a Model Dynamical System with Applications to Weak Turbulence*, Experimental Mathematics 22(3), Taylor & Francis., **250-264**, 2013, doi: 10.1080/10586458.2013.793110

[6] Dormand, J. R. and P. J. Prince, *A family of embedded Runge-Kutta formulae* J. Comp. Appl. Math., Vol. 6, **19-26**, 1980

[7] M. Guardia, *Growth of Sobolev norms in the cubic defocusing nonlinear Schrödinger equation with a convolution potential* Comm. Math. Phys., 329 (2014), no 1, **405–434**

[8] M. Guardia, V. Kaloshin *Growth of Sobolev norms in the Cubic Defocusing Nonlinear Schrödinger Equation*, Journal of the European Mathematical Society, vol. 17, 1, **71-149**, 2015

[9] T. Tao, *Nonlinear dispersive equations: Local and global analysis,* CBMS Reg. Conf. Series in Math., **106**, AMS, Providence, RI, 2006.